Structural Basis for the Functional Switch of the E. coli Ada Protein † , ‡

ARTICLE *in* BIOCHEMISTRY · MAY 2001

Impact Factor: 3.02 · DOI: 10.1021/bi002109p · Source: PubMed

Structural Basis for the Functional Switch of the *E. coli* Ada Protein[†,‡]

Yingxi Lin,[§,||] Volker Dötsch,[§,⊥] Thomas Wintner,[#,▽] Katrina Peariso,[▼] Lawrence C. Myers,[#] James E. Penner-Hahn,[▼] Gregory L. Verdine,[*,#] and Gerhard Wagner[*,§]

Department of Biological Chemistry and Molecular Pharmacology, Harvard Medical School, 240 Longwood Avenue, Boston, Massachusetts 02115, Department of Physics and Department of Chemistry and Chemical Biology, Harvard University, Cambridge, Massachusetts 02138, and Department of Chemistry, University of Michigan, Ann Arbor, Michigan 48109-1055

Received September 7, 2000; Revised Manuscript Received February 9, 2001

ABSTRACT: The *Escherichia coli* protein Ada specifically repairs the S_p diastereomer of DNA methyl phosphotriesters in DNA by direct and irreversible transfer of the methyl group to its own Cys 69 which is part of a zinc−thiolate center. The methyl transfer converts Ada into a transcriptional activator that binds sequence-specifically to promoter regions of its own gene and other methylation resistance genes. Ada thus acts as a chemosensor to activate repair mechanisms in situations of methylation damage. Here we present a highly refined solution structure of the 10 kDa N-terminal domain, N-Ada10, which reveals structural details of the nonspecific DNA interaction of N-Ada10 during the repair process and provides a basis for understanding the mechanism of the conformational switch triggered by methyl transfer. To further elucidate this, EXAFS (extended X-ray absorption fine structure) and XANES (X-ray absorption near-edge structure) data were acquired, which confirmed that the zinc−thiolate center is maintained when N-Ada is methylated. Thus, ligand exchange is not the mechanism that enhances sequence-specific DNA binding and transcriptional activation upon methylation of N-Ada. The mechanism of the switch was further elucidated by recording NOESY spectra of specifically labeled methylated-Ada/DNA complexes, which showed that the transferred methyl group makes many contacts within N-Ada but none with the DNA. This implies that methylation of N-Ada induces a structural change, which enhances the promoter affinity of a remodeled surface region that does not include the transferred methyl group.

All living organisms have developed complex systems to protect cells from the toxic effects of mutagenic chemicals and radiation. The regulation and function of DNA repair mechanisms have been characterized extensively in *Escherichia coli*. The *E. coli* protein Ada, a key player in the adaptive response of bacteria to alkylating agents, repairs the frequently occurring aberrant alkylation, especially methylation, of DNA (*1*).

The 39 kDa Ada protein has two functional domains: a 20 kDa N-terminal domain, N-Ada20,[1] which demethylates the S_p diastereomer of DNA methyl phosphotriester [MeP(s)] modifications, and a 19 kDa C-terminal domain, C-Ada19, which repairs O^6-methylguanine (O^6-MeG) and O^4-methylthymine (O^4-MeT) lesions. During these processes, the methyl groups are irreversibly transferred to Cys 69 and Cys 321, respectively (*2*−*7*). Previous studies have shown that the MeP(s) repair function is retained in the N-terminal 10 kDa domain of Ada, N-Ada10 (*3*).

A low-resolution solution structure of N-Ada10 and a crystal structure of C-Ada19 have been reported previously (*4*, *8*). Interestingly, the methylation sites in these two domains (Cys 69 and Cys 321) have different solvent accessibility. The active-site thiol of Cys 321 is buried in C-Ada19 while the thiol of Cys 69 in N-Ada10 lies near the protein surface. To explain the mechanism of methyl transfer in C-Ada19, a model has been proposed in which Cys 321

[†] This research was supported by grants (to G.W.) from the NSF (MCB 9816072) and the NIH (GM47467) and by grants (to J.E.P.-H.) from the NIH (GM-38047). Acquisition and maintenance of spectrometers and computers used for this work were supported by grants (to G.W.) from the NSF (MCB 9527181) and the Harvard Center for Structural Biology and the Giovanni Armenise−Harvard Foundation for Advanced Scientific Research. XAS measurements were made at SSRL and NSLS, which are funded by the Department of Energy, Office of Basic Energy Sciences.

[‡] Atomic coordinates have been deposited in the Protein DataBank with access code 1EYF.

* Correspondence should be addressed to G.W. [tel.: (617) 432-3213; e-mail: wagner@hms.harvard.edu] or G.L.V. [tel.: (617) 495-5323; e-mail: verdine@chemistry.harvard.edu].

[§] Department of Biological Chemistry and Molecular Pharmacology, Harvard Medical School.

[||] Department of Physics, Harvard University.

[⊥] Present address: Department of Pharmaceutical Chemistry, University of California, San Francisco, 513 Parnassus Ave., P.O. Box 0446, San Francisco, CA 94143B.

[#] Department of Chemistry and Chemical Biology, Harvard University.

[▽] Present address: Admissions Office, Williams College, Mather House, Williamstown, MA 01267.

[▼] Department of Chemistry, University of Michigan.

[1] Abbreviations: N-Ada10, N-terminal 10 kDa fragment of Ada containing residues 1−92; NMR, nuclear magnetic resonance; EXAFS, extended X-ray absorption fine structure; XANES, X-ray absorption near-edge structure; NOESY, nuclear Overhauser effect spectroscopy; N-Ada20, N-terminal 20 kDa fragment of Ada; MeP(s), S_p diastereomer of methyl phosphotriester; C-Ada19, C-terminal 19 kDa fragment of Ada; O^6-MeG, O^6-methylguanine; O^4-MeT, O^4-methylthymine; N-Ada17, N-terminal 17 kDa fragment of Ada; N-Ada16, N-terminal 16 kDa fragment of Ada; DSS, 2,2-dimethyl-2-silapentane-5-sulfonic acid; NOE, nuclear Overhauser effect; XAS, X-ray absorption spectroscopy; HSQC, heteronuclear single-quantum coherence spectroscopy; TOCSY, total correlation spectroscopy; RMSD, root-mean-square deviation.

10.1021/bi002109p CCC: $20.00
Published on Web 03/16/2001

undergoes a conformational change and becomes solvent exposed after the protein binds to its substrate (*8*).

Exposure of *E. coli* to alkylating agents stimulates increased transcription of repair proteins. This so-called adaptive response is turned on when Cys 69 is methylated by repairing an S_p methyl phosphotriester, or as a result of direct methyl transfer from alkylating agents. Ada methylated at Cys 69 becomes a strong transcriptional activator that binds to the promoter regions of genes in the Ada regulon, resulting in enhanced transcription of Ada itself and genes encoding other proteins that repair alkylation damage (*6, 7*).

This methylation-dependent sequence-specific DNA binding function is contained in N-Ada20 (*9*) and the truncated forms N-Ada16 and N-Ada17 are sufficient to maintain this function (*10*). C-Ada19, although not required for sequence-specific DNA binding, may also be involved in transcriptional activation (*11*−*14*). It has been shown that Ada, methylated at Cys 69, binds specifically to the *ada* promoter immediately upstream of the RNA polymerase binding site (*6, 15*), while the C-terminal domain may be required for direct interaction with the RNA polymerase (*6*). Mutational studies also indicate that the N- and C-terminal domains play different roles in activating *ada* transcription: methylation of Cys 69 enhances sequence-specific binding to the *ada* box (*16*) while methylation of Cys 321 enhances the transactivating capacity of the protein (*13*).

In this paper, we focus on the N-terminal 10 kDa methyl phosphotriester repair domain, N-Ada10. A preliminary solution structure of this domain was reported by Myers et al. in 1993 (*4*). It revealed a central β-sheet sandwiched between two α-helices and defined the topology of the Zn binding site. Two long surface loops were poorly defined (loop 1: 18−26, loop 2: 42−48). Subsequent NMR relaxation studies indicated that loop 1 has no higher mobility than the rest of the protein (*17*). Loop 2, which is slightly more mobile than average, was proposed to be part of the non-sequence-specific DNA binding site used during methyl phosphotriester repair. However, missing assignments for the majority of the arginine side chains in loop 2 limited the extent to which such interactions could be characterized. In addition, high-resolution structural data are needed to better understand how N-Ada interacts with methylated DNA during the process of DNA repair. Furthermore, when the structure of the complex between methylated N-Ada and the promoter DNA becomes available, a precisely defined structure of nonmethylated free N-Ada will be needed for comparison in order to understand the mechanism that converts N-Ada into a transcriptional activator.

N-Ada10 contains a tightly bound zinc ion that is required for proper protein folding (*3*). An unusual Cys-X_3-Cys-X_{26}-Cys-X_2-Cys sequence places four thiol groups, including that of the methyl recipient Cys 69, in two adjacent loops after two parallel β-strands, which allows for coordination of a zinc ion with tetrahedral geometry (*4*). The consequences of methyl transfer for the structure of the zinc−thiolate center upon methyl transfer have not yet been determined. Since methylated cysteine is likely to be a weaker zinc ligand (a thioether) than unmethylated cysteine (a thiolate), it seemed possible that it would be replaced by an alternative ligand residue upon methylation, similar to the case of matrix metalloproteases (*18*). However, an early study appears to rule out such a ligand exchange mechanism (*19*). To confirm this result, we used XANES and EXAFS studies to probe the zinc environment and average Zn−S bond length in free Ada, unmethylated Ada in complex with DNA, and a methylated Ada/DNA complex. Since methylated N-Ada10 is not stable in solution, N-Ada17 was used for these experiments.

Previous studies have shown that N-Ada10 alone has non-sequence-specific DNA binding activity, while the larger fragments N-Ada16, N-Ada17, and N-Ada20 are able to bind DNA both nonspecifically and sequence-specifically at the *ada* box (*10*). Secondary structure prediction and preliminary structural data (*20*) indicated a helix−turn−helix motif in the C-terminal part of N-Ada20, which is a common structural motif in sequence-specific DNA binding proteins. This motif seems to confer the sequence-specific binding activity upon N-Ada16 (*7*).

Methylation of Cys 69 converts N-Ada20 into a 1000-fold stronger transcriptional activator that binds to the *ada* box in a sequence-specific manner (*16*). The lack of global chemical shift perturbations upon methylation and DNA binding of N-Ada17 suggested that the methyl group might be directly involved in the protein−DNA interface (*16*). Alternatively, the transferred methyl group could be internalized in N-Ada10 or help to form the interface between the two subdomains of N-Ada17, namely, N-Ada10 and the putative C-terminal helix−turn−helix domain. Here we report NOESY spectra of selectively labeled and deuterated N-Ada17/DNA complexes, which indicate that the transferred methyl group does not make direct contact with the DNA, suggesting that methylation causes a conformational change in N-Ada10 that creates a new high-affinity DNA binding face.

MATERIALS AND METHODS

NMR Sample Preparation. Expression and purification of N-Ada10 were carried out as previously described (*3, 4*). The final NMR samples contained 1−2 mM protein in 25 mM NaH_2PO_4/Na_2HPO_4, pH 6.4, 50 mM NaCl, and 10 mM 2-mercaptoethanol. For the sequence-specific DNA binding experiments, 17 kDa fragments of Ada containing residues 1−153 (N-Ada17) were prepared and methylated at Cys 69 as described previously using either T_{11}OMe (*19*) or methyl iodide as methyl donors (*21*). In the experiments described here, perdeuterated N-Ada17 was produced by growing *E. coli* in D_2O and deuterated acetate. The degree of deuteration was checked with 1D NMR experiments as described (*22*). Subsequently, the isolated protein was methylated with $^{13}C^1H_3I$ in the presence of a 21 base pair DNA duplex with the sequence GCAAATTAAAGCGCAAGATTG. In this way, degradation of the free methylated N-Ada17 is avoided as it immediately forms a stable protein/DNA complex.

NMR Experiments and Data Analysis. NMR experiments were performed at 25 °C on Bruker AMX500 and AMX600 and Varian VXR500, UNITY500, UNITYPlus400, and UNITYPlus750 spectrometers. Pulsed field gradients and WATERGATE (*23*) were used for solvent suppression in all of the heteronuclear and most of the homonuclear experiments. In the remaining homonuclear experiments, a 1 s presaturation pulse was used for H_2O suppression. ^{13}C-filtered NOESY experiments (*24, 25*) were recorded on a Bruker 600 MHz instrument with a mixing time of 100 ms.

Data were processed on SGI computers using the Prosa (*26*) and Felix software packages (MSI, San Diego). XEASY (*27*) was used for analyzing spectra.

DSS dissolved in NMR buffer was used as an external reference to calibrate the ^{1}H chemical shifts. The ^{13}C and ^{15}N chemical shifts were calibrated from the 0 ppm ^{1}H frequency using the ratios $^{13}C/^1H = 0.25144952$ and $^{15}N/^1H = 0.10132590$, respectively (*28*).

Resonance Assignments. Nearly complete backbone and side-chain assignments were made with 3D ^{15}N-NOESY−HSQC (mixing time 100 ms), 3D ^{15}N-TOCSY−HSQC (mixing time 70 ms), 2D H_2O TOCSY (mixing time 65 ms), and 2D D_2O TOCSY (mixing time 65 ms) and HCCH-TOCSY experiments. To obtain the missing β proton assignments and remove ambiguities between β and γ resonance frequencies, we recorded a HBHA(CBCACO)-NH spectrum (*29*, *30*). Using this experiment, all of the α and β protons were assigned except for the first three and last two residues, which are presumably unstructured and show no signals in ^{15}N-HSQC spectra. Using HCCH-TOCSY experiments (*31*, *32*), almost all of the side-chain resonances could be assigned except for the γ protons of Leu 7 and Leu 84, the γ and δ protons of Arg 19, and the γ, δ, and ϵ protons of Lys 70 and Lys 86. The leucine γ protons generally overlapped with the δ protons. Furthermore, overlap in the HCCH-TOCSY spectrum prevented us from assigning the side-chain resonances of Lys 70 and Lys 86. Arg 19 gives very weak signals in ^{15}N-NOESY−HSQC and no cross-peaks beyond β protons from the Hα diagonal peak in HCCH-TOCSY. We were unable to observe the Hβ diagonal signal in HCCH-TOCSY.

We adopted the stereospecific assignments for valine and leucine methyl groups obtained from a 10% ^{13}C-labeled sample (*17*) after checking that they were consistent with other data in structure calculations. The methyl groups of Val 31 and 19 β-methylene groups were stereospecifically assigned by combining the $^3J_{H\beta_N}$ coupling constants estimated from HNHB (*33*), intraresidue NOE data, and information from the calculated structure.

Distance and Angle Restraints. NOE distance restraints were obtained using the H^N region of a 50 ms H_2O 2D NOESY and a 60 ms D_2O 2D NOESY. Longer mixing time NOESY spectra (80 and 120 ms D_2O NOESY, 100 and 150 ms H_2O NOESY) were used to confirm assignments but not for distance restraints. Peak intensities were calculated using the PEAKINT program of XEASY or, for overlapped regions, using manual elliptical integration in XEASY.

Upper limit distance restraints were generated by CALIBA (*34*). The strongest peak in the $H^\alpha-H^N$ region was set to a distance of 2.2 Å and used to calibrate the H_2O NOESY. The D_2O NOESY was calibrated using a tyrosine $H^\delta-H^\epsilon$ cross-peak set to a distance of 2.6 Å.

Φ angle restraints were determined from coupling constants, $^3J_{H\alpha_N}$, measured from an HNHA spectrum (*35*). With the exception of a few overlapped peaks that were integrated manually, all diagonal and cross-peaks were integrated using PEAKINT. The Φ angle range was restricted to −90 to −40° for $^3J_{H\alpha_N} < 5.5$ Hz, −140 to −80° for 7 Hz $< {}^3J_{H\alpha_N} <$ 9 Hz, and −140 to −100° for $^3J_{H\alpha_N} > 9$ Hz. If the NOE between an amide proton and the previous α proton was much stronger than that between the same amide proton and the intraresidue α proton, the Φ angle of that residue was restricted to −180° to 0°.

χ^1 angle restraints were determined from $^3J_{H\beta_N}$ coupling constants measured from an HNHB spectrum (*33*) and inspection of the intraresidue $H^\alpha-H^\beta$ NOEs. χ^1 angles were restrained to a ±60° range around one of the three ideal rotamer positions. Stereospecific assignments of all valine and leucine residues except Val 31 were published previously (*17*). We verified those assignments and stereospecifically assigned Val 31 and some β-methylene groups by combining the χ^1 information and the results of the structure calculations.

Constraints to enforce intramolecular hydrogen bonds were used for NH signals that were observable for at least 1 h after transfer from H_2O to D_2O at pH 6.4 and 24 °C. These constraints were only used for NH groups located in regular secondary structures and when the NOEs characteristic for the particular secondary structure were observed. With the exception of one ambiguous hydrogen bond between residue 24 and residue 27, the hydrogen bond restraints were identical to those published previously (*4*). We also used the previously published distance restraints for the zinc−thiolate center (*4*).

Structure Calculation. Structures were calculated using the distance geometry algorithm in INSIGHTII (BIOSYM Technologies, San Diego). The structure calculations were performed in several steps. First, bound smoothing was performed to satisfy triangular inequality distance limits using an extended structure with perfect bond lengths and bond angles and the distance restraints. Subsequent randomized matrization generated random distance matrices that were optimized by angular embedding and majorization in four dimensions. The final structure optimization and energy minimization were achieved by simulated annealing and conjugate gradient minimization. The initial energy used during the simulated annealing was 4500 kcal/mol. The temperature was increased from an initial value of 1 K to a maximum of 200 K with a time step size of 0.3 ps. We set the fail level for the final calculated structure to 1.0. Omega angles were allowed to vary within a 10° range.

XAS Data Analysis. XAS data were collected on methylated N-Ada17 bound to DNA at the Stanford Synchrotron Radiation Laboratory on beamline 7-3, using a Si(220) double-crystal monochromator detuned to 50% of the maximum intensity for harmonic rejection. The sample temperature was held at 10 K in an Oxford liquid helium flow cryostat during the measurements. XAS data were also collected on samples of N-Ada17, unmethylated N-Ada17 bound to DNA at the National Synchrotron Light Source (NSLS) on beamline X9B using a sagitally focused Si(111) double-crystal monochromator and a Ni-coated upstream mirror for harmonic rejection. The sample temperature was held at 16 K during data collection in a Displex cryostat. These data were measured as fluorescence excitation spectra with a 13-element Ge solid-state detector array as previously described (*36*). The energies were calibrated by simultaneous measurement of the absorption spectrum of a zinc foil and setting the first inflection point of the foil edge equal to 9659 eV.

The total and windowed count rates are given in the Supporting Information (Table S1). All of the channels from each scan were examined for the presence of glitches, and the good channels (Table S1) were then averaged to give

the final spectra. Approximately 1.3×10^6 useful counts were measured per point on methylated N-Ada17/DNA and $(3-5.0) \times 10^5$ counts per point for the other samples. The number of scans averaged for each sample are given in Table S1.

The XANES data were normalized by fitting the absorbance both below and above the edge to tabulated X-ray absorption cross sections (*37*) using a fourth-order polynomial and a single scale factor (*38*). The EXAFS background correction was performed by fitting a first-order polynomial to the pre-edge region, and a two-region cubic spline above the edge. The data were then converted to *k*-space using $k = [2m_e(E - E_0)/\hbar^2)^{1/2}$, where $E_0 = 9675$ eV. Fourier transforms were calculated using k^3 weighted data ($k = 2-12.9$ Å^{-1} for N-Ada17; $k = 2-13.6$ Å^{-1} for unmethylated N-Ada17/DNA; $k = 2-12.8$ Å^{-1} for methylated N-Ada17/DNA). The first shell ($R = 1.2-2.7$ Å for N-Ada17; $R = 1.1-3.0$ Å for unmethylated N-Ada17/DNA; $R = 1.0-2.4$ Å for methylated N-Ada17/DNA) was subsequently back-transformed over the same *k*-range. The resulting filtered data as well as the unfiltered EXAFS data were fitted to eq 1 using a nonlinear, least-squares algorithm. Filtered and unfiltered data gave equivalent structural parameters.

$$\chi(\kappa) = \sum_i \frac{N_i S_i(\kappa) A_i(\kappa)}{\kappa R_i^2} \exp(-2\kappa^2\sigma_i^2) \sin[2\kappa R_i + \phi_i(\kappa)] \quad (1)$$

EXAFS data are described by eq 1, where $\chi(\kappa)$ is the fractional modulation in the absorption coefficient above the edge, N_i is the number of scatterers at a distance R_i, $A_i(\kappa)$ is the effective backscattering amplitude, σ_i^2 is the root-mean-square variation in R_i, $\phi_i(\kappa)$ is the phase shift experienced by the photoelectron wave in passing through the potentials of the absorbing and backscattering atoms, $S_i(\kappa)$ is a scale factor specific to the absorber−scatterer pair, and the sum is taken over all scattering interactions. The program FEFF v. 6.01 (*39*, *40*) was used to calculate amplitude and phase functions, $A_i(\kappa)$ and $\phi_i(\kappa)$, for a zinc−oxygen interaction at 2.00 Å, a zinc−nitrogen interaction at 2.05 Å, and a zinc−sulfur interaction at 2.35 Å. The scale factors, $S_i(\kappa) = 1.02$ (S), 0.85 (N), and 0.90 (O), and the shift in E_0 relative to 9675 eV, $\Delta E_0 = 9$ eV, were calibrated by fitting the EXAFS data for crystallographically characterized zinc models in the case of S and N (*41*) and $[Zn(H_2O)_6]^{2+}$ for O. The individual fits were performed allowing *R* and σ to vary for each shell while holding all other parameters fixed.

RESULTS

To better understand the mechanism of the switch that converts Ada into a transcriptional activator upon methyl transfer to Cys 69, we decided to obtain a high-resolution structure of N-Ada10. A previously reported structure of N-Ada10 (*4*) had revealed the overall fold. However, due to limited spectroscopic tools which had prevented complete assignment of the protein (*17*), the structure had low precision and the putative DNA binding face was poorly defined. The extension of the assignments and the determination of a highly refined structure are steps toward the structure determination of methylated N-Ada17 in complex with the *ada*-box DNA and present a snapshot of the conformation of N-Ada prior to its methylation.

Table 1: Statistics for the Final 25 Structures

restraint type	no. of restraints
all	1014
NOE distance restraints	872
intraresidue	296
interresidue	576
sequential	200
medium range	109
i,*i*+2	38
i,*i*+3	50
i,*i*+4	21
long range	267
hydrogen bond distance restraints	46
zinc−thiolate center distance restraints	14
dihedral angle restraints	82
Φ	52
χ^1	30
mean coordinate RMSD from mean structure	
residues 8−73	
backbone heavy atoms	0.37 ± 0.050 Å
all heavy atoms	0.94 ± 0.076 Å
well-defined regions	
(residues 8−17, 27−41, and 49−69)	
backbone heavy atoms	0.27 ± 0.043 Å
all heavy atoms	0.83 ± 0.086 Å

Quality of the Refined Structure. The final errors for the 50 final calculated structures fall into 2 groups: 1 group has final errors of less than 0.3, and the other has final errors around 0.9. As will be discussed below, the larger final errors were caused by large restraint violations around the zinc−thiolate center, and this group of structures was discarded. The 25 structures in the final bundle were those structures from the first group that had no NOE violation exceeding 0.25 Å and no dihedral angle restraint violation larger than 0.7°. Statistics for the final 25 structures can be found in Table 1, which shows the high precision of the refined structure.

In the Ramachandran plot for residues 5−75 of the 25 final structures (not shown), more than 80% of the angles are within the most favorable region, and the rest are in the additionally allowed region. We also calculated the number of interresidue distances less than 3 Å in the final ensemble of structures: 137 of the expected 201 short distances were present in our distance restraints, and NOEs corresponding to the remaining 64 short distances were not identified primarily due to overlap in the 2D NOESY spectra.

Figures 1a and 1b show the number of NOE restraints and coordinate RMSDs for each residue, revealing the expected inverse correlation. The RMSD is very low except for the N- and C-termini. Apart from residues 24 and 25, which undergo conformational exchange (see below), all of the residues in the structured portion of the protein (residues 8−73) have well-defined dihedral angles with angular order parameters (*42*) greater than 0.9 for their Φ and Ψ angles (Figure 1).

Description of the Refined Structure. N-Ada10 contains one central β-sheet sandwiched between two α-helices (Figure 2). The ordered structure begins with a long helix, H1 (residues 8−18). Two β-turns, a type I turn at residues 20−23 and a type II turn at residues 23−26, connect H1 to the first β-strand, β1. β1(27−31), β2(36−39), β3(52−55),

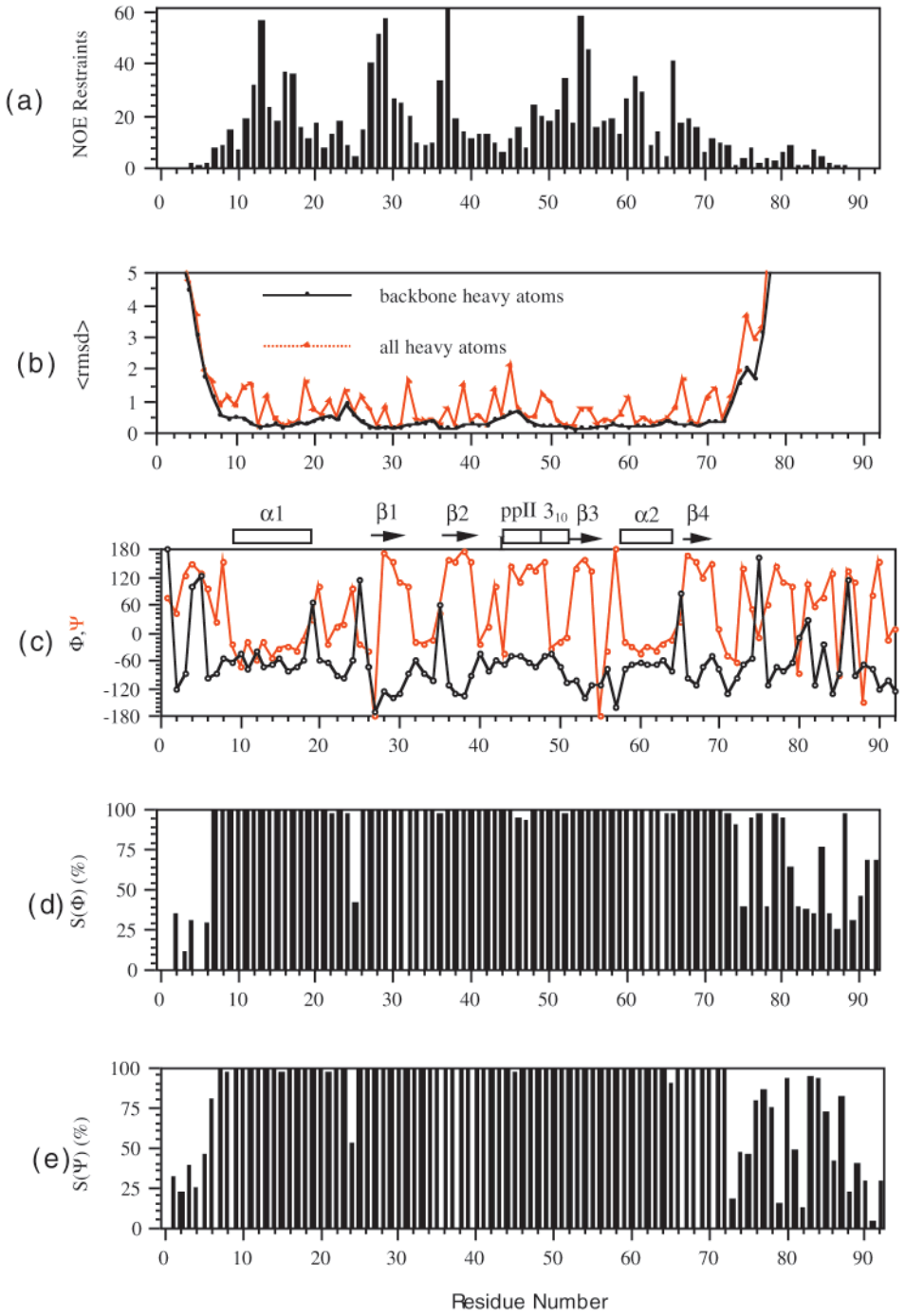

FIGURE 1: Statistics for the final ensemble of 25 structures. (a) Number of NOE distance restraints per residue. (b) Coordinate RMSD from the mean structure for each residue in the final ensemble. (c) Mean Φ and Ψ angles. At the top of the panel, the secondary structure is shown with arrows for β-strands and open boxes for helices. The poly-proline helix is labeled ppII. (d) Angular order parameters (*42*) of the Φ angles. (e) Angular order parameters of the Ψ angles.

and β4(66−69) pack against each other such that β1, β2, and β3 are antiparallel and β4 and β2 are parallel. A type I β-turn at residues 32−35 connects β1 and β2 while part of the loop between β2 and β3 forms a poly-proline type II (ppII) helix (44−47) and a short 3_{10} helix (48−51). The second helix, H2 (58−64), crosses three of the β-strands to bring β4 alongside β2 and has an N-cap hydrogen bond from the Asn 57 side-chain $O^{\delta}1$ to the backbone amide proton of Ser 59.

The largest changes upon refinement of the structure involve loop 1 (residues 18−26). This loop is now well-defined, and a previously indicated 3_{10} helix was not confirmed (*4*). The low Φ and ψ angular order parameters (*42*) of residues Asp 24 and Gly 25 (Figure 1d,e) could be the result of multiple conformations. Consistent with this, the amide proton of Gly 25 in the 2D NOESY and 3D ^{15}N-NOESY−HSQC spectra has two adjacent signals, indicating conformational exchange that is slow on the NMR time scale. The very high *R*2/*R*1 value for Gly 25 found during relaxation studies (*17*) confirms the presence of conformational and/or solvent exchange at this position.

The refinement also affected the definition of the structure of residues 42−48, which are close to the metal center and seem to be part of the DNA binding face. This region, which

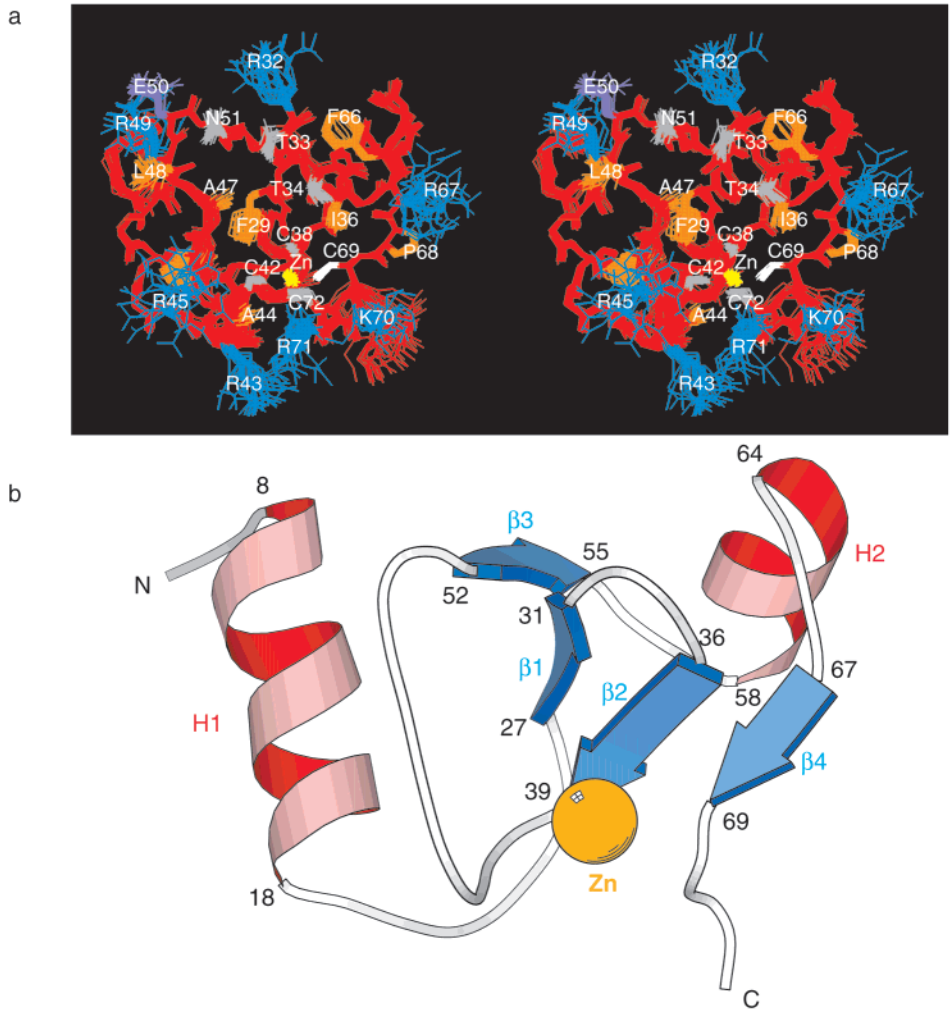

FIGURE 2: (a) Stereoview of the ensemble of 25 structures (backbone of residues 5−75 and the zinc atom), generated using InsightII (MSI, San Diego). Side chains on the surface around the zinc−thiolate center are shown: positive side chains are in blue, negative side chains in purple, polar side chains in gray, and hydrophobic side chains in orange. The zinc atom is shown in yellow and the side chain of Cys 69 in white. (b) Ribbon diagram of the structure with the smallest final error. The orientation is the same as in (a). This figure was generated using Molscript (*49*).

appeared to be disordered in the preliminary structure, is now well-defined. Numerous new NOE cross-peaks in this region showed that this segment contains a poly-proline type II helix and a 3_{10} helix. Nevertheless, this region is still slightly less well-defined than the rest of the protein, which is consistent with the results of relaxation studies (*17*).

To precisely define the state of Ada prior to methylation and the conformational change that converts the protein into a transcriptional activator, we have attempted to define side-chain orientations of surface residues, in particular for the putative DNA binding face. This will be crucial for comparison with the structure of the complex with DNA once this becomes available. Figure 2a displays the ensemble of calculated structures including the side chains of all residues in the putative DNA binding face. This face has highly conserved surface residues at residue positions 33−36, 45, 51, and 66−71. Besides the four cysteines that coordinate the zinc (Cys 38, Cys 42, Cys 69, Cys 72), Thr 34, Gly 35, Asn 51, Phe 66, Arg 67, Lys 70, and Arg 71 are absolutely conserved (*2*). For Thr 33, a serine substitution is found in one homologue, conserving the hydroxyl group, and Arg 45 is replaced by a lysine in one homologue. Ile 36 and Pro 68 are replaced by other hydrophobic residues (valine and alanine). The side-chain orientation of all of these residues is very well-defined, except for the lysines and arginines, which are mobile beyond the C^{β} atoms (Figure 2a).

The Zinc−Thiolate Center. The zinc−thiolate center is located at the bottom of a cavity on the protein surface, and each sulfur atom is partially exposed to the solvent (Figure 3). Furthermore, Cys 69 is situated on the rim of this cavity and is therefore available to contact the methyl group, consistent with its role as the methyl acceptor. The four cysteine ligands are in the *S* configuration (*43*). The structure calculations produced a number of conformations containing the *R* configuration, but these models exhibited large restraint violations around the zinc−thiolate center and large values of the target function (see above). They were not considered further in our analysis. The structural details of the zinc−thiolate center of N-Ada10 are different from those of other known zinc sites in proteins. We compared the conformation around the zinc center with those of the GATA and GR protein families (*44*), which also have *S* configurations. No similarity in the backbone or side-chain conformations was found. Furthermore, there are no characteristic hydrogen bonds to the cysteine thiolate sulfur atoms, a feature that has been reported for proteins with CCHC and other zinc

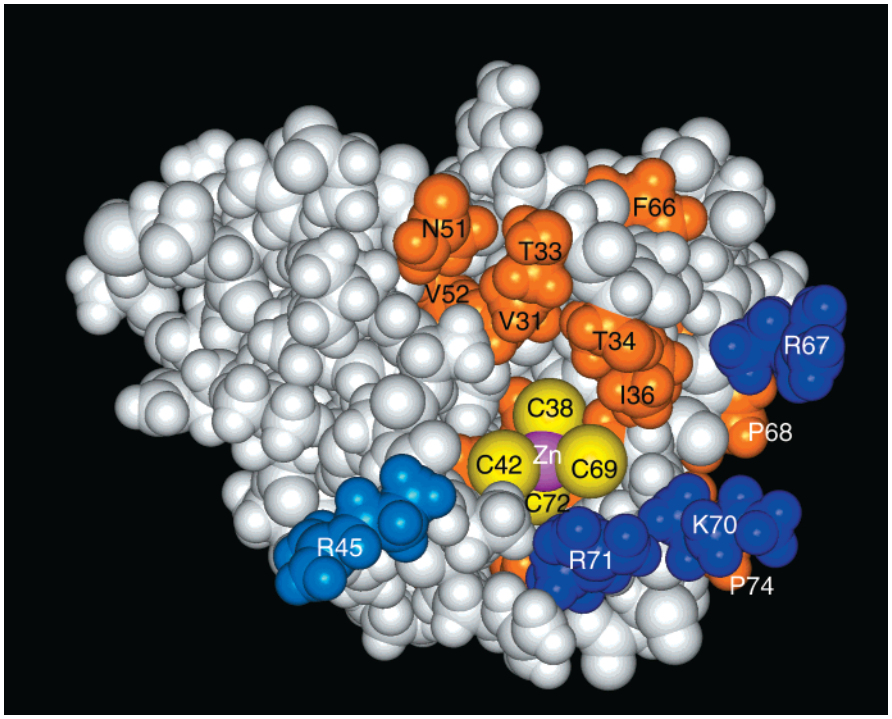

FIGURE 3: Space filling model of N-Ada10 (residues 5−75) showing the surface around the zinc−thiolate center. The orientation is the same as in Figure 2. The zinc atom is shown in magenta, and the sulfurs of cysteine residues are in yellow. Strictly conserved basic side chains are shown in dark blue, the highly conserved basic side chain of Arg 45 in blue, and other conserved side chains in orange. This figure was produced with InsightII (MSI, San Diego).

binding motifs (*45*). No potential hydrogen bond donor is close enough to the sulfur atoms to form a hydrogen bond (Figure 3). It seems that formation of such hydrogen bonds is observed for proteins where the zinc plays a structural role, perhaps protecting the metal from solvent access. In the case of Ada, the zinc−thiolate center has to be accessible for methyl transfer, and formation of hydrogen bonds between the sulfur atoms and other protein groups might inhibit this process.

Does Methylation Cause a Change in Zinc Ligation? To explore whether methylation and DNA binding affect the structure around the zinc site, we recorded XANES and EXAFS spectra of free N-Ada17, a complex of nonmethylated N-Ada17 with DNA, and a complex of methylated N-Ada17 with DNA (Figure 4). XANES and EXAFS spectra of the free protein and the unmethylated N-Ada17/DNA complex are essentially superimposable, demonstrating that binding of Ada to DNA does not cause a detectable change in the zinc site. The amplitude of the main peak in both Fourier transforms is comparable to that seen for zinc tetrathiolate models, consistent with the expected zinc ligation. Fits to the EXAFS data confirm this interpretation: all of the EXAFS spectra for unmethylated Ada are best modeled as a tetrathiolate zinc site with a Zn−S distance of 2.36 Å (Table 2). In contrast, both the XANES and EXAFS for methylated N-Ada17/DNA show significant changes relative to unmethylated protein, indicating a change at the Zn site. The XANES spectrum of methylated N-Ada17/DNA shows a new feature at ~9670 eV and an overall broadening of the spectrum between 9660 and 9680 eV. The EXAFS data also point to a change in zinc ligation. There is a dramatic decrease in amplitude of the main peak in the Fourier transform, and this peak shifts to a shorter distance. Quantitative fits confirm that there is a change in zinc

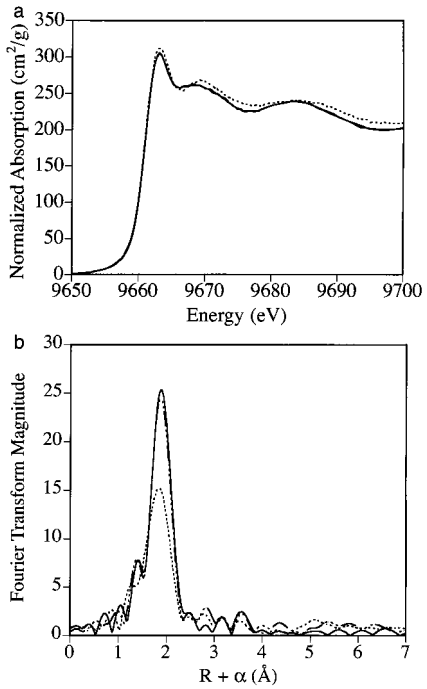

FIGURE 4: (a) Zn XANES spectra of N-Ada17 (solid line), N-Ada17/DNA complex (dot−dash line), and methylated N-Ada17/DNA complex (dotted line). (b) Fourier transforms of the Zn EXAFS data for N-Ada17 (solid line), N-Ada17/DNA complex (dot−dash line), and methylated N-Ada17/DNA complex (dotted line).

ligation. The EXAFS data for methylated N-Ada17/DNA can be modeled as a ZnS_3 site. However, the observed Zn−S bond distance is 2.32 Å, a distance consistent with a 4-coordinate Zn site [the Zn−S distances in crystallographically characterized zinc trithiolates are ~2.23 Å (*41*)].

Table 2: EXAFS Fits for the Ada Protein[a]

	CN	R_{ab} (Å)	$\sigma^2 \times 10^3$ (Å^2)	CN	R_{ab} (Å)	$\sigma^2 \times 10^3$ (Å^2)	F' [b]
N-Ada17[a]	3S	2.36	2.4				0.051
	4S	2.36	3.9				0.030
	3S	2.36	2.8	1O	2.21	2.9	0.028
unmethylated	3S	2.36	2.4				0.040
N-Ada17	4S	2.36	4.0				0.036
/DNA	3S	2.36	2.47	1O	2.11	5.6	0.029
methylated	3S	2.32	5.7				0.026
N-Ada17	3S	2.32	5.7	1O	2.15	11.5	0.018
/DNA	3S	2.32	5.4	1S	2.52	29.4	0.028

[a] All fits were calculated for filtered EXAFS data. Fits to unfiltered data gave identical parameters with higher *F*-values due to the inclusion of additional noise in the data. [b] $F = \left|\frac{K^6(data\ fit)^2/N}{(N_{dof} - N_{var})}\right|$; $N_{dof} = \frac{2\Delta\kappa\Delta R}{\pi}$.

Thus, the average Zn−S distance decreases by 0.04 Å when Ada is methylated. Often a decrease in distance is due to a decrease in coordination number, since the remaining ligands form stronger bonds to compensate. However, a decrease of 0.04 Å is less than expected for a change from 4- to 3-coordinate, suggesting that the fourth ligand, Cys 69, has not been lost, but rather has been replaced with a weaker ligand. This weaker ligand could be either the thioether of the methylcysteine or H_2O if the methylated Cys is displaced from the Zn altogether.

It is difficult to define the EXAFS for one weak ligand in the presence of three strong ligands, thus making it difficult to distinguish between these possibilities. The protocol that we have developed for fitting for mixed ligand (S+N/O) systems (*41*) does not give chemically realistic values for methylated Ada. The Debye−Waller factors are too large in comparison with model compounds, and the apparent Zn−(O/N) distance is too long (2.15 Å) in comparison with crystallographically characterized ZnS_3O models (*46, 47*). These observations indicate that the Zn in methylated Ada is not coordinated to three thiolates and one oxygen. In contrast, the data can be well modeled with a shell of 3S at 2.32 Å and 1S at 2.52 Å. The long Zn−S interaction has a large Debye−Waller factor, as expected for a weak, distant interaction. The 2.52 Å distance is reasonable for a Zn−thioether interaction, and the bond−valence−sum calculations for the four distances together (3S at 2.32 Å + 1S at 2.52 Å) are consistent with divalent Zn. The EXAFS data for methylated Ada are thus most consistent with the ligation of the Zn by three thiolate sulfurs and one thioether sulfur at long distance. Zinc coordination by a thioether has also been observed in farnesyltransferase (*48*). Our result is consistent with an independent study, which showed the existence of $^{113}Cd-^{13}C$ coupling in the ^{113}Cd-bound form of the methylated N-Ada17 between the cadmium atom and the carbon atom of the transferred methyl group, indicating a lack of ligand exchange during methylation of Ada (*19*).

Does the Transferred Methyl Group Contact the DNA during Sequence-Specific Binding? To determine whether the transferred methyl group is directly involved in the DNA interaction or causes a structural rearrangement of N-Ada, we prepared a methylated N-Ada17/DNA complex with a ^{13}C label in the transferred methyl group using methods described previously (*16*). The ^{13}C-filtered NOESY spectrum of this complex revealed many NOEs to the methyl group, indicating that it makes a large number of contacts (Figure 5a). To determine whether these contacts involved the bound DNA or the Ada protein itself, we prepared a methylated N-Ada17/DNA complex containing 100% deuterated protein and a protonated ^{13}C-labeled methyl group transferred to Cys 69. This was expected to remove all NOE cross-peaks from the methyl group to the protein, and leave only cross-peaks to the DNA. The experiment was performed in D_2O to eliminate cross-peaks to exchangeable protons. Surprisingly, the NOESY spectrum of this complex, recorded repeatedly, showed no NOEs at all (Figure 5b). This indicates that the transferred methyl group does not contact the DNA and makes contacts only within the Ada protein.

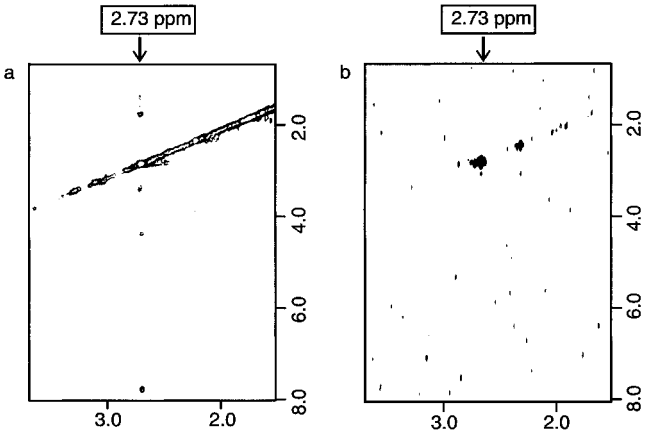

FIGURE 5: 2D ^{13}C-filtered NOESY spectra recorded of (a) a methylated complex in which both protein and DNA are unlabeled and protonated, but the transferred methyl group is ^{13}C labeled, and (b) the same as (a) but the protein is 100% deuterated except for the transferred methyl group. Both samples in D_2O. The mixing time used in these experiments is 100 ms.

DISCUSSION

N-Ada10 specifically demethylates the S_p diastereomer of DNA methyl phosphotriesters, which indicates its ability to recognize the S_p diastereomer of the methylated phosphate group and bind non-sequence-specifically to DNA. The refined structure we present provides new insights into the underlying molecular recognition mechanism. N-Ada seems to interact with DNA in two different ways: a DNA sequence-independent binding prior to methylation repair and a sequence-specific binding after methylation. The change in DNA binding specificity, which converts Ada into a 1000-fold stronger sequence-specific DNA binder and a transcriptional activator, is crucial to Ada's functions as a chemosensor and adapter. The data we present here provide a clear structural basis for the mechanism of Ada's functional switch.

DNA Binding of N-Ada10 and Structure of the Methyl Sensor. To repair MeP(s) DNA, N-Ada10 must bind to methylated DNA in a mode that is independent of the DNA sequence. This suggests that recognition of the negatively charged phosphate backbone of DNA is crucial for this interaction. The distribution of charged residues on the surface of N-Ada10 creates a striking polarity of the electrostatic potential (Figure 6). The basic residues on the positive face of the protein are likely to facilitate the initial interaction of the negatively charged DNA with N-Ada and may be responsible for orienting the two molecules relative to each other in a way that is optimal for methyl transfer.

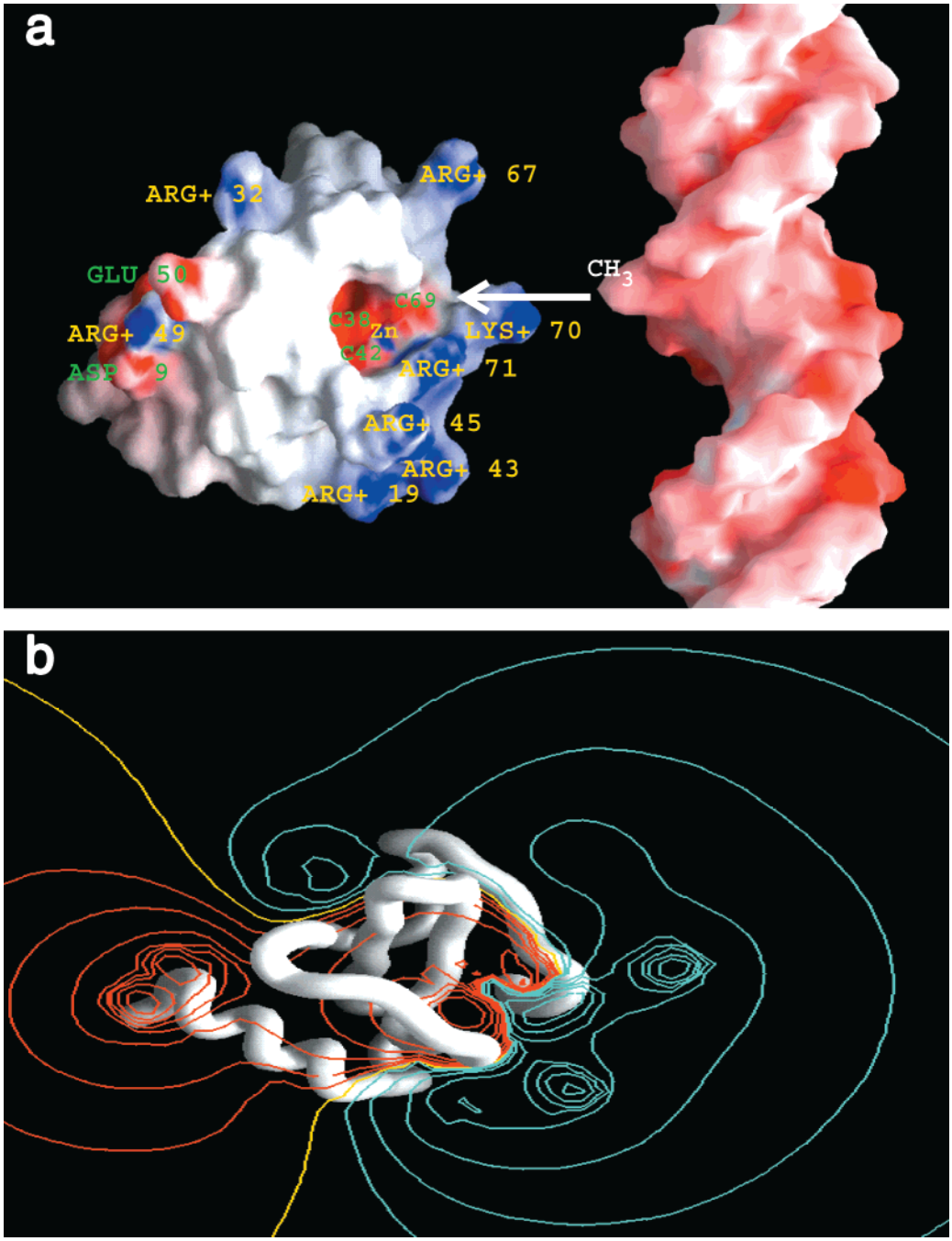

FIGURE 6: (a) Protein surface of N-Ada10 (residues 5−75) colored according to the electrostatic potential calculated with the program GRASP (*50*). Blue represents positive potential and red negative. To the right is a model of B-DNA bearing a methylated phosphotriester. (b) Protein backbone worm in the same orientation as (a) with a contour plot of the 3D isoelectrical potential projected onto the plane of the paper, also generated by GRASP (*50*). The yellow line indicates zero potential. Blue lines show positive potentials of 0.5, 1.0, 2.0, 4.0, 8.0, 16.0, 32.0, and 64.0 kT. Red lines show negative potentials of the same magnitude.

Most of the basic side chains, in particular the conserved ones, are clustered around the zinc−thiolate center. They are located on two parallel ridges next to the hydrophobic groove containing the active-site cysteine (residue 69). Arg 43, Arg 45, Leu 48, and Cys 69, whose backbone chemical shifts have previously been shown to be perturbed by DNA binding (*4*), are all on this face of the protein (Figure 6a). Furthermore, the highly refined structure presented here reveals a remarkable cavity in the surface of N-Ada10 (Figure 6a). At the bottom of this cavity is the zinc ion. The sulfur of the methyl acceptor Cys 69 is located at the rim of the cavity (Figure 6a). This surface conformation forms a "methyl trap" that is complementary in shape to the methylated phosphate on DNA. Figure 6a shows a model of methylated B-DNA in a position where the protruding methyl group can be inserted into the cavity. The cavity is large enough to accommodate the methylated phosphate group so that the phosphate oxygen can approach the sulfur of Cys 69 for the methyl transfer to occur.

How Does Methylation Induce Sequence-Specific DNA Binding? The data we present indicate that the integrity of the zinc−thiolate center is preserved in methylated N-Ada17, indicating that ligand exchange is not involved in the structural switch that converts Ada into a transcriptional

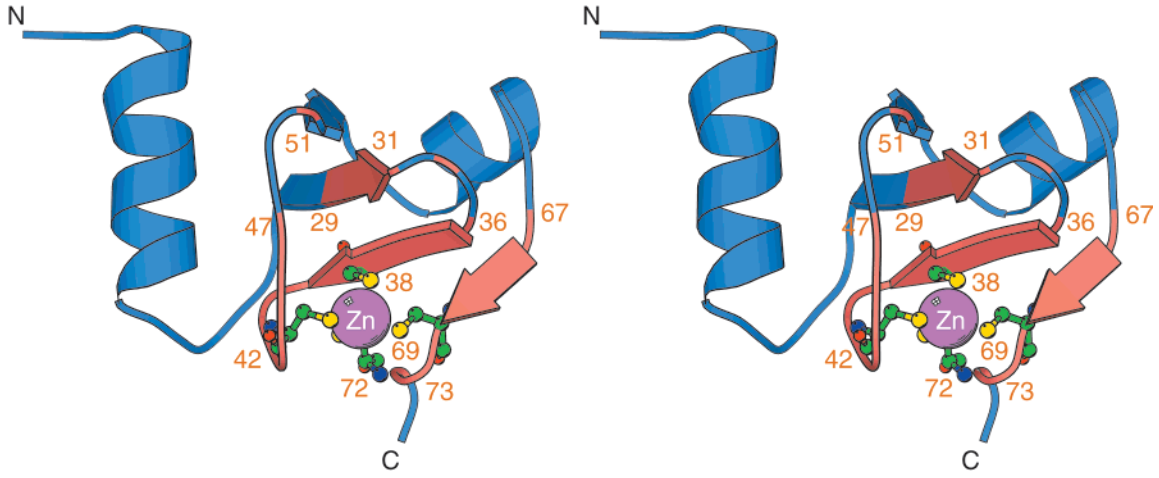

FIGURE 7: Region of N-Ada10 that may undergo a conformational change induced by methylation at Cys 69. Residues showing significant chemical shift perturbations ($|\Delta\delta H| > 0.1$ ppm or $|\Delta\delta N| > 1$ ppm) upon methylation of N-Ada16 are colored in salmon red and other residues in blue. Side chains of the four cysteine ligands are shown and colored by atom type. The zinc atom is in magenta. This figure was produced with Molscript (*49*).

activator. However, the bond between the zinc and the sulfur atom in the methylated cysteine becomes weaker, as indicated by the EXAFS data. It remains to be seen whether the weakening of this bond has functional importance.

What does the existence of contacts between the transferred methyl group and the protein imply about the effect of methylation on the structure and function of N-Ada20? One possibility is that the transferred methyl group makes contact with the C-terminal helix−turn−helix motif, thereby stabilizing the association of the two subdomains (connected by a flexible, unstructured linker) to form a composite DNA binding surface. However, such a possibility is not very likely, based on the observation that methylation of Cys69 causes backbone amide chemical shift changes in the N-terminal 10 kDa domain but not in the helix−turn−helix motif in the C-terminal part of N-Ada16 (*20*). This suggests that the methyl group makes contact only with N-Ada10 itself, suggesting a model in which the transferred methyl group remains "trapped" in the cavity described above. Consistent with this, Figure 7 shows the chemical shift changes that occur upon methylation mapped onto the surface of the refined structure of N-Ada10. The changes are concentrated around the cavity on one face of the protein, in the vicinity of Cys 69 (compare Figure 6a and Figure 7). These changes could be the result of spontaneous loss of Zn^{2+} upon methylation, but seem likely to be caused by methylation-dependent conformational rearrangements in the N-Ada10 domain alone. These structural changes could serve to position key residues in N-Ada10 for interaction with DNA. Consistent with this idea, Sakashita and co-workers have reported that binding of methylated N-Ada16 to the *ada* box DNA caused chemical shift changes in the same region around Cys 69, as well as in the helix−turn−helix motif.

When these results are combined with the fact that the transferred methyl group contacts the protein only, it is clear that the methyl group must reside in the cavity inside the N-terminal 10 kDa domain of Ada. The cavity above the zinc atom (Figure 6a) may allow the methyl group to enter the protein's interior and make contact with residues in the hydrophobic core. It is likely that the methyl transfer closes the cavity of the "methyl trap" (Figure 6a), and the remodeled protein surface is directly involved in making contact with the DNA during sequence-specific binding. Thus, methylation of Ada creates a new DNA binding surface in the 10 kDa N-terminal domain that is responsible for the 1000-fold increase in sequence-specific DNA binding affinity and transcripntional activation function.

ACKNOWLEDGMENT

We thank Mr. G. Heffron for assistance with NMR spectroscopy, Dr. P. Zhou for fruitful discussions, and Dr. C. M. Fletcher for suggestions and critical reading of the manuscript.

SUPPORTING INFORMATION AVAILABLE

A table with the EXAFS data collection parameters (1 page). This material is available free of charge via the Internet at http://pubs.acs.org.

REFERENCES

1. Teo, I., Sedgwick, B., Demple, B., Li, B., and Lindahl, T. (1984) *EMBO J. 3*, 2151−2157.
2. Hakura, A., Morimoto, K., Sofuni, T., and Nohmi, T. (1991) *J. Bacteriol. 173*, 3663−3672.
3. Myers, L. C., Terranova, M. P., Nash, H. M., Markus, M. A., and Verdine, G. L. (1992) *Biochemistry 31*, 4541−4547.
4. Myers, L. C., Verdine, G. L., and Wagner, G. (1993b) *Biochemistry 32*, 14089−14094.
5. Myers, L. C., Terranova, M. P., Ferentz, A. E., Wagner, G., and Verdine, G. L. (1993a) *Science 261*, 1164−1167.
6. Sedgwick, B., Robins, P., Totty, N., and Lindahl, T. (1988) *J. Biol. Chem. 263*, 4430−4433.
7. Sakashita, H., Sakuma, T., Ohkubo, T., Kainosho, M., Sakumi, K., Sekiguchi, M., and Morikawa, K. (1993) *FEBS Lett. 323*, 252−256.
8. Moore, M. H., Gulbis, J. M., Dodson, E. J., Demple, B., and Moody, P. C. E. (1994) *EMBO J. 13*, 1495−1501.
9. Lindahl, T., Sedgwick, B., Sekiguchi, M., and Nakabeppu, Y. (1988) *Annu. Rev. Biochem. 57*, 133−157.
10. Akimaru, H., Sakumi, K., Yoshikai, T., Anai, M., and Sekiguchi, M. (1990) *J. Mol. Biol. 216*, 261−273.
11. Saget, B. M., and Walker, G. C. (1994) *Proc. Natl. Acad. Sci. U.S.A. 91*, 9730−9734.
12. Saget, B. M., Shevell, D. E., and Walker, G. C. (1995) *J. Bacteriol. 177*, 1268−1274.

13. Taketomi, A., Nakabeppu, Y., Ihara, K., Hart, D. J., Furuichi, M., and Sekiguchi, M. (1996) *Mol. Gen. Genet. 250*, 523−532.
14. Swindells, M. B. (1993) *FEBS Lett. 323*, 257−260.
15. Teo, I., Sedgwick, B., Kilpatrick, M. W., McCarthy, T. V., and Lindahl, T. (1986) *Cell 45*, 315−324.
16. Myers, L. C., Jackow, F., and Verdine, G. L. (1995) *J. Biol. Chem. 270*, 6664−6670.
17. Habazettl, J., Myers, L. C., Yuan, F., Verdine, G. L., and Wagner, G. (1996) *Biochemistry 35*, 9335−9348.
18. Springman, E. B., Angleton, E. L., Birkedal-Hansen, H., and Van Wart, H. E. (1990) *Proc. Natl. Acad. Sci. U.S.A. 87*, 364−368.
19. Myers, L. C., Cushing, T. D., Wagner, G., and Verdine, G. L. (1994) *Chem. Biol. 1*, 91−97.
20. Sakashita, H., Sakuma, T., Akitomo, Y., Ohkubo, T., Kainosho, M., Sekiguchi, M., and Morikawa, K. (1995) *J. Biochem. (Tokyo) 118*, 1184−1191.
21. Myers, L. C., Wagner, G., and Verdine, G. L. (1995) *J. Am. Chem. Soc. 117*, 10749−10750.
22. Walters, K. J., Matsuo, H., and Wagner, G. (1996) *J. Am. Chem. Soc. 119*, 5958−5959.
23. Piotto, M., Saudek, V., and Sklenar, V. (1992) *J. Biomol. NMR 2*, 661−665.
24. Otting, G., Senn, H., Wagner, G., and Wüthrich, K. (1986) *J. Magn. Reson. 70*, 500−505.
25. Otting, G., and Wüthrich, K. (1990) *Q. Rev. Biophys. 23*, 39−96.
26. Güntert, P., Dötsch, V., Wider, G., and Wüthrich, K. (1992) *J. Biomol. NMR 2*, 619−629.
27. Bartels, C., Xia, T., Billeter, M., Güntert, P., and Wüthrich, K. (1994) *J. Biomol. NMR 5*, 1−10.
28. Cavanagh, J., Fairbrother, W. J., Palmer, A. G., III, and Skelton, N. J. (1996) *Protein NMR spectroscopy: principles and practice*, Academic Press, Inc., San Diego.
29. Grzesiek, S., and Bax, A. (1993) *J. Biomol. NMR 3*, 185−204.
30. Grzesiek, S., and Bax, A. (1992) *J. Am. Chem. Soc. 114*, 6291−6293.
31. Bax, A., Clore, G. M., and Gronenborn, A. M. (1990) *J. Magn. Reson. 88*, 425−431.
32. Kay, L. E., Xu, G., Singer, A. U., Muhandiram, D. R., and Forman-Kay, J. D. (1993) *J. Magn. Reson. B101*, 333−337.
33. Archer, S. J., Ikura, M., Torchia, D. A., and Bax, A. (1991) *J. Magn. Reson. 95*, 636−641.
34. Güntert, P., Braun, W., Billeter, M., and Wüthrich, K. (1989) *J. Am. Chem. Soc. 111*, 3997−4004.
35. Vuister, G. W., and Bax, A. (1993) *J. Am. Chem. Soc. 115*, 7772−7777.
36. Peariso, K., Goulding, C. W., Huang, S., Matthews, R. G., and Penner-Hahn, J. E. (1998) *J. Am. Chem. Soc. 120*, 8410−8416.
37. McMaster, W. H., Del Grande, N. K., Mallett, J. H., and Hubbell, J. H. (1969) U.S. Department of Commerce Report Number UCRL-50174-SEC 2-R1.
38. Waldo, G. S. (1991) Ph.D. Thesis, University of Michigan.
39. Rehr, J. J., de le Mustre, J., Zabinsky, S. I., and Albers, R. C. (1991) *J. Am. Chem. Soc. 113*, 5135−5140.
40. Rehr, J. J., Albers, R. C., and Zabinsky, S. I. (1992) *Phys. Rev. Lett. 69*, 3397−3400.
41. Clark-Baldwin, K., Tierney, D. L., Govindaswamy, N., Gruff, E. S., Kim, C., Berg, J., Koch, S. A., and Penner-Hahn, J. E. (1998) *J. Am. Chem. Soc. 120*, 8401−8409.
42. Hyberts, S. G., Goldberg, M. S., Havel, T. F., and Wagner, G. (1992) *Protein Sci. 1*, 736−751.
43. Berg, J. M. (1988) *Proc. Natl. Acad. Sci. U.S.A. 85*, 99−102.
44. Omichinski, J. G., Clore, G. M., Schaad, O., Felsenfeld, G., Trainor, C., Appella, E., Stahl, S. J., and Gronenborn, A. M. (1993) *Science 261*, 438−446.
45. Klein, D. J., Johnson, P. E., Zollars, E. S., De Guzman, R. N., and Summers, M. F. (2000) *Biochemistry 39*, 1604−1612.
46. Dance, I. G. (1980) *J. Am. Chem. Soc. 102*, 3445−3451.
47. Mizobe, Y., Hosomizu, M., and Hidai, M. (1998) *Inorg. Chim. Acta 273*, 238−243.
48. Huang, C. C., Casey, P. J., and Fierke, C. A. (1997) *J. Biol. Chem. 272*, 20−23.
49. Kraulis, P. J. (1991) *J. Appl. Crystallogr. 24*, 946−950.
50. Nicholls, A., Sharp, K. A., and Honig, B. (1991) *Proteins: Struct., Funct., Genet. 11*, 281−296.

BI002109P